Beam steering and signal amplification through feedforward networks Part I Transmission

Tyler Levasseur[a],* Antonio Palacios[b],† and Visarath In[c‡]
[a] *Kochava Inc., Sandpoint, ID 83864, USA*
[b] *Nonlinear Dynamical Systems Group, Department of Mathematics, San Diego State University, San Diego, CA 92182*
[c] *Naval Information Warfare Center Pacific, Code 71740, 53560 Hull Street, San Diego, CA 92152-5001, USA*
(Dated: June 8, 2021)

Conventional and modern methods for beam steering in antennas and radar systems have one goal in common: to manipulate the phase shift between oscillating components, so that the direction of a radiating intensity pattern can be controlled. Typical components include arrays of nonlinear oscillators connected in a chain configuration. Modern methods for beam steering take advantage of the inherent nonlinearities of the individual components and of the collective dynamics of the array of oscillators to successfully manipulate phase shift. None of those methods include, however, signal amplification. In this manuscript, we introduce a novel array configuration: a feedforward network, which allows, simultaneously, for beam steering and signal amplification capabilities.

PACS numbers: 05.40.+j, 02.50.Ey, 85.25.Dq

I. INTRODUCTION

Beam steering is about manipulating the direction of a radiating far-field intensity pattern. Applications usually include: optics, acoustics, and, antenna and radar systems. In optics, for instance, beam steering can be done by either changing the refracting index of the medium through which the beam is transmitted or by the use of mirrors, prisms, or rotating diffraction gratings. In acoustics, beam steering is about changing the direction of audio from speakers, and it can be accomplished by changing the magnitude and phase of speakers arranged in an array. In antennas and radar systems, beam steering can be achieved either by switching the antenna elements or by controlling the phase differences between oscillating components, which typically consist of arrays of nonlinear oscillators.

It has been shown [1] that the far-field intensity pattern of an antenna or radar system consists of alternating light and dark bands, also known as *interference fringes*. These interference fringes arise from the phase differences incurred by the different path lengths between the sources. When a constant phase shift between neighboring sources is introduced, then the positions of the interference fringes, and, consequently, the radiating pattern, will change. Thus, controlling the phase shift between nonlinear oscillators is of critical importance for achieving beam steering. Common methods for controlling the phase differences of the nonlinear oscillators include: phase shifters [2], injection current [3, 4], and frequency de-tuning [5, 6]. Conventional phase shifters act on individual oscillators but they have limitations due to power loss and size constraints for on-chip implementations. Injection current involves applying a current to the end elements of the array, which, in turn, leads to a uniform phase gradient. This approach requires for the individual elements to be designed to match the frequency of the injected signal. A significant drawback of this approach is the fact that the steering range decreases as a function of the array size. Last but not least, frequency de-tuning takes advantage of the inherent collective behavior of the array. This method seeks to achieve synchronization of an entire array of oscillators with a particular phase gradient through carefully tuning the frequencies of the two end-elements of the array. None of these techniques include, however, signal amplification.

In this manuscript, we are interested in developing the theory for a novel mechanism for beam steering for antennas and radar systems. Novel in the sense that we employ a feedforward network of nonlinear oscillators, instead of the common chain array that other schemes have used [5, 7, 8], to accomplish, simultaneously, beam steering and signal amplification. A feedforward network is a unidirectionally coupled chain of dynamical systems in which the first cell is coupled to itself, and each successive cell is coupled to the next one. Feedforward networks have gained considerable interest [9–12] because of their potential to enhance signal amplification. In this manuscript we show that a feedforward network approach can yield both features, control of phase gradient and signal amplification. In part I, we consider the *transmission problem*: generating and steering the radiating patterns that emanate from the sources. In part II, we consider the *reception problem*: understanding the response of the nonlinear beamformer to incident signals and noise. The manuscript is organized as follows. In Section II, a review

*Electronic address: tylerslevasseur@gmail.com
†Electronic address: apalacios@sdsu.edu
‡Electronic address: visarath@spawar.navy.mil

of the most common approach to beam steering through frequency de-tuning is discussed. In addition, the fundamental ideas of feedforward networks and their collective response are briefly introduced. Empirical simulations show that feedforward networks have the ability to produce, through the collective interactions of the nodes, signal amplification. In Section III we employ asymptotic methods (e.g., two-time scale analysis) to investigate the dynamics of a feedforward network and their collective response for beam steering and signal amplification.

II. BACKGROUND

In this section we provide a review of basic ideas of beam steering and of the phenomenology of feedforward networks. In the former case, we describe, mathematically, the formation of the radiating beam pattern, and how it can be changed by changing the constant phase shift between neighboring sources. In the latter case, we review signal amplification through Hopf bifurcations in feedforward networks. More specifically, in a standard Hopf bifurcation, the amplitude of the ensuing oscillations scales as the square-root from the distance of the Hopf bifurcation point. In a feedforward network, the scaling follows, however, a sixth-root power. A sixth-root scaling can lead to significant signal amplification near the onset of the bifurcation.

A. BEAM STEERING

Common point sources for beam steering in active antennas and radar systems consist of multiple nonlinear oscillators, e.g., van der Pol oscillators, each driving a separate radiation patch element. The oscillators are usually arranged in an array, as is shown in Fig. 1.

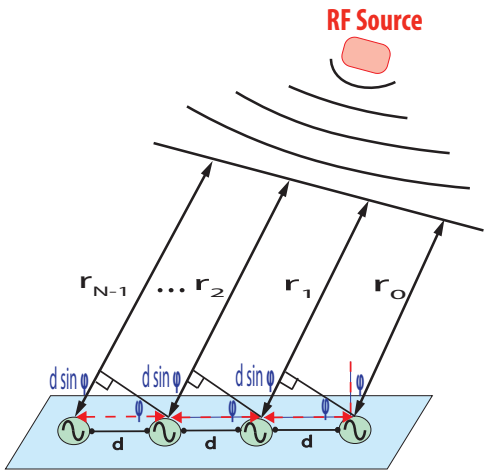

FIG. 1: An array of nonlinear oscillators drive individual radiation elements to form a radiation beam pattern.

The radiation produced by each patch element has both an (assumed to be identical) amplitude, E_0, and a phase, $\xi_j = \vec{k}\cdot\vec{r}_j$, where $\vec{k}$ is the free-space wave vector, and $\vec{r}_j$ is the position vector from the j^{th} radiation element to some observation point P. When N of these signals interact with one another, they can collectively produce a total radiation field pattern. When P is far away from the array, the total radiating electric field is

$$E(P) = \frac{1}{N}\sum_{j=0}^{N-1} E_0 e^{i\xi_j} = \frac{1}{N}\sum_{j=0}^{N-1} E_0 e^{i\vec{k}\cdot\vec{r}_j}. \qquad (1)$$

Figure 1 shows that for points in the far-field, i.e., for distances from the elements much grater than the array size $(N-1)d$, the wave vector and the position vector are, approximately, parallel, so that $\vec{k}\cdot\vec{r}_j \approx kr_j$. Equation (1) can then be re-written as

$$E(P) = \left(\frac{1}{N}\sum_{j=0}^{N-1} e^{ik(r_j - r_1)}\right) E_0 e^{ikr_1}. \qquad (2)$$

Since $r_j - r_1 = jd\sin\varphi$, where φ is the angle of incidence or transmission of the radiation wave, we can, once again, re-write Eq. (2) as

$$E(P) = \left(\frac{1}{N}\sum_{j=0}^{N-1} e^{ijkd\sin\varphi}\right) E_0 e^{ikr_1}. \qquad (3)$$

Equation (3) is also known as the *array pattern multiplication property*. It indicates that the total radiation pattern of an antenna array is the product of the electric field produced by a single patch element, $E_0 e^{ikr_1}$, multiplied by an *Array Factor*, $A(\Psi)$, which is the term in parenthesis written as

$$A(\Psi) = \frac{1}{N}\sum_{j=0}^{N-1} e^{ij\Psi}, \qquad (4)$$

where $\Psi = kd\sin\varphi$. Direct calculations show that the array factor given by Eq. (4) can also be expressed as

$$A(\Psi) = \frac{\sin\left(\frac{N\Psi}{2}\right)}{N\sin\left(\frac{\Psi}{2}\right)} e^{i(N-1)\Psi/2}. \qquad (5)$$

Figure 2 shows the array factor for an array antenna with $N = 8$ elements, plotted in rectangular and polar coordinates. Observe that $|A(\Psi)|$ is symmetric with respect to $\Psi = 0$, and it always attains a maximum at $\Psi = 0$, which corresponds to an angle of incidence of $\varphi = 0$. This angle is also known as the *broadside direction* as it is normal to the plane of the array. Notice also that the width of the main lobe decreases as N increases.

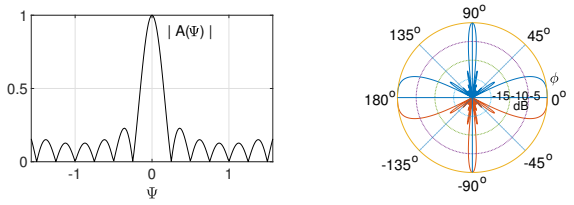

FIG. 2: Array factor for an array antenna with $N = 8$ identical elements, plotted in (top) rectangular coordinates and (bottom) polar coordinates.

We now seek to make the connection between the phase, ϕ_j, of each nonlinear oscillator and that of the radiating pattern of an active antenna. Individual oscillators are usually coupled to one another bidirectionally, so that the dynamics of an array, of size N, is governed by the following system of differential equations, written in normal form

$$\dot{z}_j = (\alpha + \omega_j i)\, z_j - |z_j|^2 z_j + \kappa e^{i\Phi}(z_{j+1} - 2z_j + z_{j-1}) + f_e(t), \tag{6}$$

where z_j is a complex-valued state variable for each oscillator j, with $j = 1, \ldots, N$, with boundary conditions $z_0 = z_{N+1} = 0$, α is the main excitation bifurcation parameter, which determines the amplitude of the ensuing oscillations, ω_i is related to the natural frequency of each oscillator, κ is the coupling strength among nearest neighbors, Φ is a coupling phase parameter, and $f_e(t)$ is an external incoming signal, usually of the form $f_e(t) = a(t)e^{i(\Omega t+\varphi)}$, where $a(t)$ is a complex amplitude factor that allows for slow changes (relative to the oscillating period) in the magnitude or phase, φ, of the incoming signal, with frequency Ω.

When $f_e(t) = 0$, the antenna operates in *transmission* mode, while when $f_e(t) \neq 0$ then the antenna functions as a receiver. In the former case, the emphasis is on the radiating patterns that emanate from the sources. The latter case concerns the response of the nonlinear beamformer to incident signals and noise. In both cases, transmission and receiving, one seeks solutions to the model Eq. (6) with a spatially uniform phase gradient across the array, i.e., in the form

$$z_j(t) = A_j e^{i\phi_j(t)}. \tag{7}$$

Previous calculations of the total radiating electric field assume the radiating source elements to be in-phase. Assuming now a uniform phase gradient across the array, introduced by the individual phase of the oscillators, such that

$$\xi_j = kr_j + \phi_j.$$

Substituting ξ_j into Eq. (1), while assuming a constant phase difference among neighboring oscillators, i.e., $\phi_{j+1} - \phi_j = \theta$, so that $\phi_j - \phi_1 = j\theta$, then a similar set of calculations yield

$$E(P) = \left(\frac{1}{N}\sum_{j=0}^{N-1} e^{ij(kd\sin\varphi+\theta)}\right) E_0 e^{i(kr_1+\phi_1)}. \tag{8}$$

It follows that the array factor becomes

$$A(\Psi+\theta) = \frac{\sin\left(\dfrac{N(\Psi+\theta)}{2}\right)}{N\sin\left(\dfrac{\Psi+\theta}{2}\right)} e^{i(N-1)(\Psi+\theta)/2}. \tag{9}$$

Consequently, the constant phase difference among the oscillators leads to a shift or steering of the beam pattern, from the angle Ψ to $\Psi+\theta$. Figure 3 illustrates the effect of steering the beam pattern shown in Fig. 2 by a constant phase difference of $\theta = -60^0$.

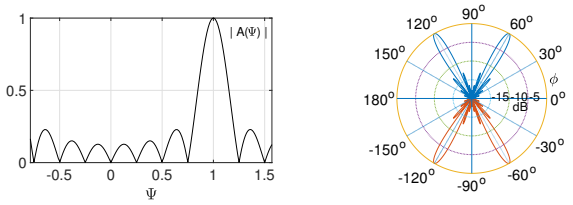

FIG. 3: Array factor for an array antenna with $N = 8$ identical elements, steered by an angle of -60^0, plotted in (top) rectangular coordinates and (bottom) polar coordinates.

Now, assume the phase of each individual oscillator to be defined as

$$\phi_j = \omega t + (j-1)\theta.$$

Substituting the desired solution (7), i.e., $z_j(t) = A_j e^{i\omega t+(j-1)\theta}$ into the model Eq. (6), and assuming identical amplitudes of oscillations, where, $E_0 = A_j$, yields the following conditions on the natural frequencies:

$$\begin{aligned} \omega_1 &= \omega + \kappa\sin(\theta+\Phi) \\ \omega_j &= \omega + (j-1)\dot{\theta} \\ \omega_N &= \omega + (N-1)\dot{\theta} - \kappa\sin(\theta+\Phi). \end{aligned} \tag{10}$$

In the *static* approach to beam steering, phase differences must be controlled so that the array produces a stationary far-field pattern at a fixed location. This case implies that $\dot{\theta} = 0$. It follows that the natural frequencies of only the two end elements, ω_1 and ω_N, need to be manipulated. By contrast, in the *dynamic* approach, one seeks a far-field intensity pattern that moves continuously. In this case, $\dot{\theta} \neq 0$, which implies that to achieve a continuously scanning beam then the natural frequency of every individual oscillator must be adjusted in a time-dependent manner [5, 7, 8].

B. FEEDFORWARD NETWORKS

Feedforward networks are a specific type of network characterized by a homogeneous chain of unidirectionally coupled nodes. The first node may or may not be self-coupled; we examine both cases here. The unidirectional coupling prevents feedback in the system, so that one system may influence another without being itself affected. We show that under the right conditions, the feedforward network causes certain bifurcations to exhibit accelerated growth rates.

The normal form [11, 13, 14] for a Hopf bifurcation is given by Eq. (11).

$$\dot{z} = (\mu + \omega i)\, z - (1 + \gamma i)|z|^2 z. \tag{11}$$

For $\mu > 0$, the origin loses stability and tends to oscillate at frequency ω with some positive amplitude. For $\mu < 0$, the origin is a stable equilibrium and the cell will tend to zero. Equation (11) is the *normal form* of a Hopf bifurcation, and therefore this is the simplest possible system which displays a Hopf bifurcation.

Consider, for example, the three-cell feedforward network shown in Fig. 4. The internal dynamics of each cell is governed by a Hopf bifurcation as in (11).

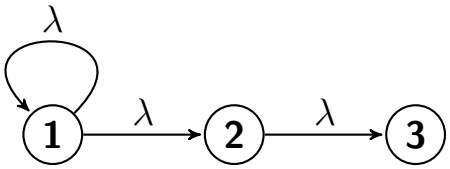

FIG. 4: Representative example of a three-cell feedforward network. Arrows indicate coupling, with coupling strength λ. Each cell represents a dynamical system assumed to be operating near a Hopf bifurcation.

The network is then modeled by the following system of equations

$$\begin{aligned}
\dot{z}_1 &= (\mu + i\omega)\, z_1 - (1 + i\,\gamma)\, |z_1|^2\, z_1 - \lambda z_1 \\
\dot{z}_2 &= (\mu + i\omega)\, z_2 - (1 + i\,\gamma)\, |z_2|^2\, z_2 - \lambda z_1 \\
\dot{z}_3 &= (\mu + i\omega)\, z_3 - (1 + i\,\gamma)\, |z_3|^2\, z_3 - \lambda z_2.
\end{aligned} \tag{12}$$

The authors in [9–11] have found that the coupling causes the amplitudes of oscillation that arise from the onset of the Hopf bifurcation to grow at a larger rate. If μ is the bifurcation parameter, and $\mu = 0$ is the onset of a supercritical Hopf bifurcation, then the third cell undergoes oscillations of amplitude approximately equal to $\mu^{1/6}$, rather than the *expected* amplitude of $\mu^{1/2}$. This phenomenon showcases an accelerated growth rate that has the potential for the design and fabrication of advanced filters in signal processing [15, 16]). An example of a time series, obtained from simulations of Eq. (12), which exhibits this growth phenomenon is shown in Fig. 5.

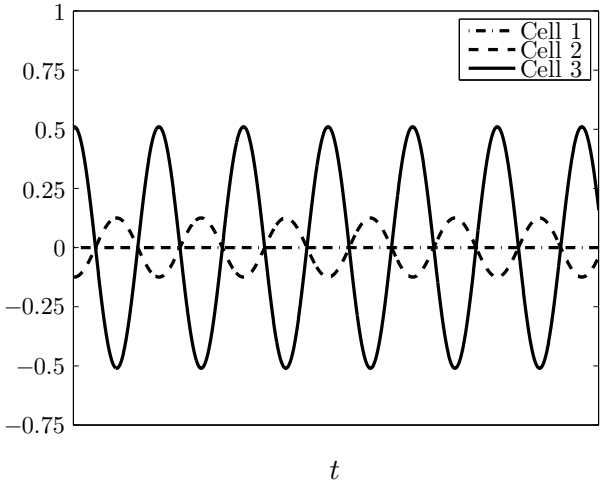

FIG. 5: Amplitude of oscillations produced by the onset of a Hopf bifurcations in the feedforward network shown in Fig. 4. Parameters are: $\mu = (1/2)^{1/6}$, $\omega = 1$, $\gamma = 0$, $\lambda = 1$. Observe the signal amplification effect on the third cell.

As the feedforward network grows in size, the authors report that the growth rate of oscillations in the final cell are determined by taking successive cube roots [15]. Thus, in a five-cell feedforward network, the growth rate should be proportional to the 54^{th} root of the bifurcation parameter, which has also been proved in [17]. This is exciting indeed, and has strayed a long way from the simple square-root growth rate. This, of course, means that large amplitude oscillations may arise very soon after the onset of the Hopf bifurcation.

This phenomenon of such large-amplitude oscillations in the third cell can be understood as a type of nonlinear resonance as well as being the result of the combination of the unidirectional coupling and the higher-degree nonlinearities [12]. Due to the network topology of the feedforward network, the third (or last) oscillator is being periodically forced by the previous one. This line of inquiry led to investigations of periodically forced Hopf bifurcations, and even periodically forced feedforward networks of Hopf bifurcations [11, 15, 18]. Related articles, proving anomalous growth rates can occur for equilibria in (unusual) regular networks, for bifurcations at simple eigenvalues are in [19, 20].

In the next two sections we explore, analytically and computationally, a feedforward network approach for generating and steering a radiation beam pattern with the extra feature of signal amplification. Individual oscillators are assumed to be governed by the normal forms for a Hopf bifurcation, as in Eq. (11), with $\gamma = 0$. Van der Pol oscillators, in particular, fall within this category. Then, depending on how the first oscillator is coupled, two versions of a feedforward network can be designed. One where the first oscillator is self-coupled, as it appears in Eq. (12), and a second version, where self-coupling is removed. Both cases are considered in these sections.

III. FEEDFORWARD NETWORK WITH SELF COUPLING

In this section we consider a feedforward network approach (with self coupling) for addressing the transmission problem, i.e., for generating and steering a radiation pattern. When the first oscillator in the feedforward network is coupled to itself, the model equations take the form

$$\begin{aligned} \dot{z}_1 &= (\alpha + \omega_1 i)\, z_1 - |z_1|^2 z_1 - \kappa e^{i\Phi} z_1 \\ \dot{z}_j &= (\alpha + \omega_j i)\, z_j - |z_j|^2 z_j - \kappa e^{i\Phi} z_{j-1}, \end{aligned} \tag{13}$$

where $j = 1, \ldots, N$, κ is the coupling strength, Φ is a coupling phase parameter. Figure 6 illustrates the potential of using a feedforward network for beam steering and signal amplification. Observe that the network oscillates in a collective phase-locking pattern. The first cell does not oscillate, while the second cell oscillates with an amplitude proportional to the square root of the bifurcation parameter α. This is typical behavior of a Hopf bifurcation. The third cell, and subsequent cells, oscillate, however, with a larger growth of $1/6^{\text{th}}$ root of α. The signal amplification on the third, and following cells, is very promising.

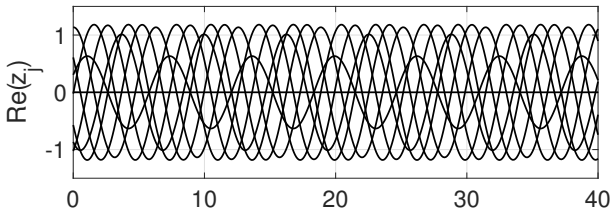

FIG. 6: Collective response of a feedforward network of $N = 8$ van der Pol oscillators. Without incoming external signal, the oscillators phase lock. Observe that the first node of the network does not oscillate, while the second node oscillates with an amplitude proportional to the square root of the bifurcation parameter α. The third cell, and subsequent cells, oscillate, however, with a larger growth of $1/6^{\text{th}}$ root of α. Parameters are: $\alpha = 0.4$, $\omega_j = 1.0$, $\kappa = 1.0$, and $\Phi = \pi/3$.

A. Signal Amplification

We now investigate the collective response of the feedforward network Eq. (13). To get insight into the mechanism for signal amplification, we consider, first, $N = 3$ oscillators. Later on we will generalize some of the results to larger networks. We write the model equations in the following form:

$$\begin{aligned} \dot{x} &= (\alpha + i\omega_0)x - |x|^2 x - \kappa e^{i\Phi} x \\ \dot{y} &= (\alpha + i\omega_0)y - |y|^2 y - \kappa e^{i\Phi} x \\ \dot{z} &= (\alpha + i\omega_0)z - |z|^2 z - \kappa e^{i\Phi} y. \end{aligned} \tag{14}$$

We note that the self-coupling in the first cell changes its effective growth and frequency parameter considerably. Indeed, since the dynamics of the first cell decouples from that of the others, we can re-write its governing equation as

$$\dot{x} = ((\alpha - \kappa\cos\Phi) + (\omega_0 - \kappa\sin\Phi)\, i)\, x - |x|^2 x, \tag{15}$$

which shows that the effective natural frequency of the first cell is different from that of the subsequent oscillators down the network. This also implies that the bifurcation parameter in the first cell is different than the bifurcation parameters of the second and third cells.

In order to determine an asymptotic expansion for x, y, and z, uniformly valid for large times, we introduce two time scales: a fast time, $\xi = \omega t$, and a slow time $\eta = \varepsilon t$, where

$$\omega = \omega_0 - \varepsilon\kappa\sin\Phi.$$

Applying the chain rule we can conclude that

$$\frac{d}{dt} = \omega_0 \frac{\partial}{\partial \xi} - \varepsilon\kappa\sin\Phi \frac{\partial}{\partial \xi} + \varepsilon \frac{\partial}{\partial \eta}. \tag{16}$$

We seek to suppress exponential growth, nonlinearities, and couplings through an asymptotic expansion for x, y, and z in a truncated series of ε of the form

$$\begin{aligned} x &= x_0 + \varepsilon x_1 + \varepsilon^2 x_2 + \cdots \\ y &= y_0 + \varepsilon y_1 + \varepsilon^2 y_2 + \cdots \\ z &= z_0 + \varepsilon z_1 + \varepsilon^2 z_2 + \cdots . \end{aligned} \tag{17}$$

Substituting Eq. (17) into Eq. (14), and using Eq. (16), produces, after collecting equal powers of ε, a set of partial differential equations (PDE) for each order term. For brevity, the technical details of the derivation of the PDEs up to $\mathcal{O}(\varepsilon)$, are shown in Appendix A. The solutions of the PDEs yields

$$\begin{aligned} x_0 &= A(\eta) e^{i(\xi + \phi_1(\eta))} \\ y_0 &= B(\eta) e^{i(\xi + \phi_2(\eta))} \\ z_0 &= C(\eta) e^{i(\xi + \phi_3(\eta))}, \end{aligned} \tag{18}$$

where the amplitudes A, B, and C, and phases, are governed by the following system of differential equations:

$$\begin{aligned} A' &= \alpha A - A^3 - \kappa A\cos\Phi \\ B' &= \alpha B - B^3 - \kappa A\cos(\Phi - \phi_2) \\ C' &= \alpha C - C^3 - \kappa B\cos(\Phi - (\phi_3 - \phi_2)) \\ \phi_1' &= 0 \\ \phi_2' &= \kappa\sin\Phi - \kappa\frac{A}{B}\sin(\Phi - \phi_2) \\ \phi_3' &= \kappa\sin\Phi - \kappa\frac{B}{C}\sin(\Phi - (\phi_3 - \phi_2)). \end{aligned} \tag{19}$$

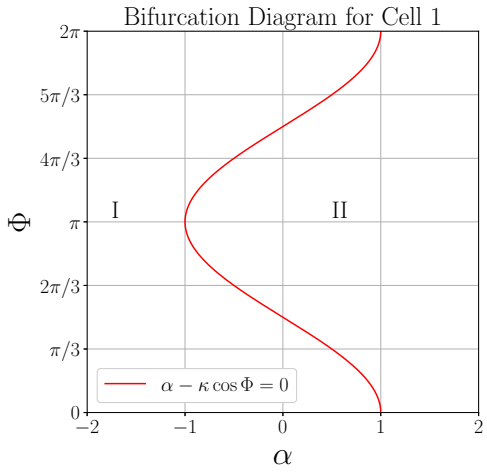

FIG. 7: Locus of Hopf bifurcation associated with oscillations in the first cell of a three-cell feedforward network. Coupling strength: $\kappa = 1$. Region I has a stable equilibrium point at $A = 0$, i.e., no oscillations exist. Region II has two stable equilibrium points at $A = \pm\sqrt{\alpha - \kappa\cos\Phi}$, which represent the amplitude of stable limit cycle oscillations. Since A is an amplitude, we only consider the positive square root. Region II also contains the trivial equilibrium but it's unstable.

1. *First Cell*

Let us consider the dynamics of just the first cell of the feedforward network. Two good reasons for singling this cell out are: it is the only cell to be self-coupled; and, in a feedforward network, the first cell can have an extreme impact on the behavior of the rest of the network. From Eq. (19) we get

$$\begin{aligned} A' &= (\alpha - \kappa\cos\Phi)\, A - A^3 \\ \phi_1' &= 0. \end{aligned} \tag{20}$$

Observe from Eq. (20) that we may simply consider $\phi_1 = 0$ as a point of reference for the phase of the oscillations in the first cell. Substituting $\phi_1 = 0$ into Eq. (18) we get a solution to order ε^0 for x_0:

$$x_0 = Ae^{i\xi} = Ae^{i\omega t}.$$

It follows that x_0 undergoes limit cycle oscillations at a frequency $\omega = \omega_0 - \varepsilon\kappa\sin\Phi$. The oscillations emerge through the locus of a Hopf bifurcation given by

$$\alpha - \kappa\cos\Phi = 0. \tag{21}$$

The locus of the Hopf bifurcation separates the parameter space (α, Φ) into two regions, which are illustrated in Fig. 7.

In Region I, $\alpha - \kappa\cos\Phi < 0$, thus only the trivial equilibrium point, $A = 0$, exists. The linearization of Eq. (20) about this equilibrium point yields

$$\dot{\delta}_A = (\alpha - \kappa\cos\Phi)\delta_A,$$

where δ_A is a small perturbation. Since $\alpha - \kappa\cos\Phi < 0$, then $\delta_A \to 0$ as $t \to \infty$. It follows that the trivial equilibrium is locally asymptotically stable. No oscillations are possible in Region I.

In Region II, $\alpha - \kappa\cos\Phi > 0$, thus there are now three equilibrium points. Since A is an amplitude, we will require that $A \geq 0$, so we can assume two possible equilibrium points: $A_1 = 0$ or $A_2 = \sqrt{\alpha - \kappa\cos\Phi}$. The linearization of Eq. (20) about $A_1 = 0$ now shows $\delta_{A_1} \to \infty$, as $t \to \infty$. Thus the trivial equilibrium becomes unstable. The linearization about the nontrivial equilibrium yields

$$\dot{\delta}_A = -2(\alpha - \kappa\cos\Phi)\delta_A.$$

Since $\alpha - \kappa\cos\Phi > 0$ then the perturbation decays, i.e., $\delta_A \to 0$ as $t \to \infty$. It follows that the nontrivial equilibrium is stable, and, consequently, cell one oscillates with amplitude $A_2 = \sqrt{\alpha - \kappa\cos\Phi}$.

When $\kappa = 1$ and $\pi/2 \leq \Phi \leq 3\pi/2$, the locus of the Hopf bifurcation appears at values of $\alpha < 0$, as it can be seen in Fig. 7(top). This produces qualitatively different behavior than the one we have studied in previous work [12]. In that work we observed the first cell to undergo a Hopf bifurcation for *larger* values of α, as opposed to lesser values. Thus we may now observe behavior where the first cell has undergone a Hopf bifurcation and the following cells have not. At the end of this section, we conduct further analysis of this situation and show that this Hopf bifurcation is associated with a synchronization state, in which all cells oscillate with the same waveform and same phase. Conditions for the existence and stability of the synchronization state are also studied.

When $\kappa = -1$, the locus of the Hopf bifurcation is just the mirror reflection of the one observed in Fig. 7 with $\kappa = 1$. As in that case, the locus (not shown for brevity) divides the parameter space (α, Φ) into two regions. One where only the stable trivial equilibrium exists, and one with a stable limit cycle oscillations.

2. *Second Cell*

Now we consider the dynamics of the second cell. From Eq. (19), we get

$$\begin{aligned} B' &= \alpha B - B^3 - \kappa A\cos(\Phi - \phi_2) \\ B\phi_2' &= \kappa B\sin\Phi - \kappa A\sin(\Phi - \phi_2). \end{aligned} \tag{22}$$

System (22) is an asymptotically autonomous system. Note: a system $\dot{x} = f(x,t)$ is asymptotically autonomous if $f(x,t) \to g(x)$ as $t \to \infty$. In this case, B is a function of A, which itself is a function of time whose dynamics are

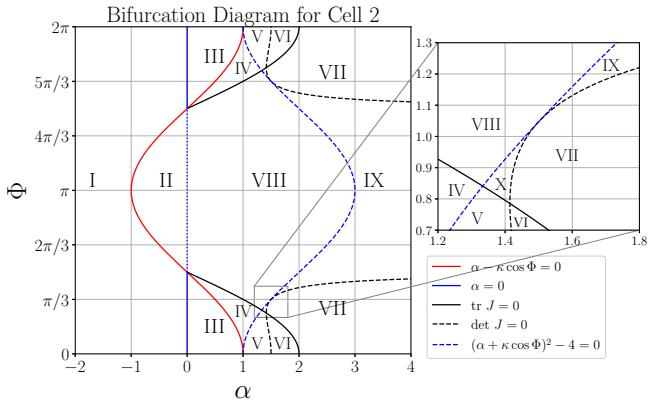

FIG. 8: Two parameter bifurcation diagram for the dynamics of the second cell in a three-cell feedforward network with coupling strength $\kappa = 1$. Ten different regions of parameter space (α, Φ), can be observed. Synchronized oscillations (i.e., same wave form and phase) occurs within Regions II, VIII, IX and X.

not governed by Eq. (22). Since A always converges to an equilibrium point, the dependence of B on A vanishes as A becomes indistinguishable from a constant. Theorem 17.0.3 in Wiggins [13] makes this precise, and allows us to consider the different cases for the long-term behavior of A.

Consider the case $\alpha - \kappa\cos\Phi \leq 0$. In this situation, we may assume $A = 0$. Then Eq. (22) becomes

$$\begin{aligned} B' &= \alpha B - B^3 \\ \phi_2' &= \kappa \sin\Phi. \end{aligned} \tag{23}$$

Observe that this is the normal form of a supercritical Hopf bifurcation. The solution $B = 0$ is stable when $\alpha \leq 0$ and, since we are assuming $\alpha - \kappa\cos\Phi \leq 0$, then $B = 0$ exists and is stable within region Region I of Fig. 8. Additionally, stable branches $B = \pm\sqrt{\alpha}$ exist along with the unstable branch $B = 0$ when $\alpha > 0$, which leads to Region III.

We can solve the second equation of Eq. (23) to get

$$\phi_2(\eta) = \kappa \sin(\Phi)\eta. \tag{24}$$

Substituting Eq. (24) into Eq. (44), we find

$$y_0 = Be^{i(\xi + \kappa\sin(\Phi)\eta)} = Be^{i(\omega t + \varepsilon\kappa\sin(\Phi)t)} = Be^{i\omega_0 t}. \tag{25}$$

It follows then that the second cell undergoes oscillations with frequency ω_0.

Consider now the case $\alpha - \kappa\cos\Phi > 0$. This case leads to a more rich dynamics than the previous one. We examine and describe in brief terms some of the collective dynamics observed throughout Regions II and IV - X. A complete analysis of all these regions is beyond the scope of the present work. We may assume $A = \sqrt{\alpha - \kappa\cos\Phi}$. We could also assume $A = 0$, which is the unstable branch of solutions of A, which leads the analysis back to Eq. (23), i.e., to the well-understood supercritical Hopf bifurcation. Such solutions exist, but are unstable. Substituting then the stable branch of solutions of A into Eq. (22) yields

$$\begin{aligned} B' &= \alpha B - B^3 - \kappa\sqrt{\alpha - \kappa\cos\Phi}\cos(\Phi - \phi_2) \\ B\phi_2' &= \kappa B\sin\Phi - \kappa\sqrt{\alpha - \kappa\cos\Phi}\sin(\Phi - \phi_2). \end{aligned} \tag{26}$$

One may readily verify that (B^*, ϕ_2^*) is an equilibrium point of Eq. (26), where $B^* = \sqrt{\alpha - \kappa\cos\Phi}$ and $\phi_2^* = 0$. The Jacobian matrix for the linearization of Eq. (26) about the equilibrium (B^*, ϕ_2^*) yields

$$J_{(B^*,\phi_2^*)} = \begin{pmatrix} -2\alpha + 3\kappa\cos\Phi & -\kappa\sqrt{\alpha - \kappa\cos\Phi}\sin\Phi \\ \dfrac{\kappa\sin\Phi}{\sqrt{\alpha - \kappa\cos\Phi}} & \kappa\cos\Phi \end{pmatrix}. \tag{27}$$

The eigenvalues of this Jacobian matrix are:

$$\sigma = \frac{1}{2}\mathrm{tr}\, J \pm \frac{1}{2}\sqrt{\Delta},$$

where

$$\begin{aligned} \mathrm{tr}\, J &= -2\alpha + 4\kappa\cos\Phi \\ \det J &= -2\alpha\kappa\cos\Phi + 2\kappa^2\cos^2\Phi + \kappa^2, \end{aligned}$$

and $\Delta = (\mathrm{tr}\, J^2) - 4\det J = 4(\alpha - \kappa\cos\Phi)^2 - 4\kappa^2\sin^2\Phi$. The synchronization state exists when the condition $\alpha - \kappa\cos\Phi > 0$ is satisfied, while its stability is guaranteed when, in addition, $\mathrm{tr}\, J < 0$, and $\det J > 0$. To identify the common region of parameter space, (α, Φ), where these conditions are satisfied, we plot the boundary curves: $\mathrm{tr}\, J = 0$ and $\det J = 0$, as well as $\alpha - \kappa\cos\Phi = 0$. In this way, we obtain the bifurcation diagram shown in Fig. 8. It follows that the synchronization state exists and is stable within Regions II, VIII, IX, and X. In this last Region X, bistability between the synchronization state and a phase-locked solution is found. Which solution is observed, depends on the initial conditions, i.e., on the basins of attraction of each individual solution.

Returning to Eq. (26), assuming that an equilibrium point exists, we arrive (via the Pythagorean theorem) at the identity

$$B^2\left(\alpha - B^2\right)^2 + \kappa^2 B^2\sin^2\Phi = \kappa^2\left(\alpha - \kappa\cos\Phi\right). \tag{28}$$

Eq. (28) can be factored into

$$\left(B^2 - (\alpha - \kappa\cos\Phi)\right)\left(B^4 - B^2\left(\alpha + \kappa\cos\Phi\right) + 1\right) = 0, \tag{29}$$

which implies that $B = \sqrt{\alpha - \kappa\cos\Phi}$ is always a solution. The other term is quadratic in B^2, which has solutions when $\left(\alpha + \kappa\cos\Phi\right)^2 - 4 \geq 0$. The emergence of these solutions results in saddle node bifurcations along the locus of the solutions of $\left(\alpha + \kappa\cos\Phi\right)^2 - 4 = 0$.

We can also determine the different branches of solutions that arise in B by factoring Eq. (28).

$$\begin{aligned}
&\text{Branch 1: } B = \sqrt{\alpha - \kappa\cos\Phi} \\
&\text{Branch 2: } B = \sqrt{\frac{\alpha + \kappa\cos\Phi + \sqrt{(\alpha+\kappa\cos\Phi)^2 - 4}}{2}} \\
&\text{Branch 3: } B = \sqrt{\frac{\alpha + \kappa\cos\Phi - \sqrt{(\alpha+\kappa\cos\Phi)^2 - 4}}{2}}.
\end{aligned} \tag{30}$$

Figure 9 illustrates the different branches of solutions for the second cell. Observe that, in Region III, the amplitude of the oscillations along the second cell follow the standard square root growth associated with a Hopf bifurcation.

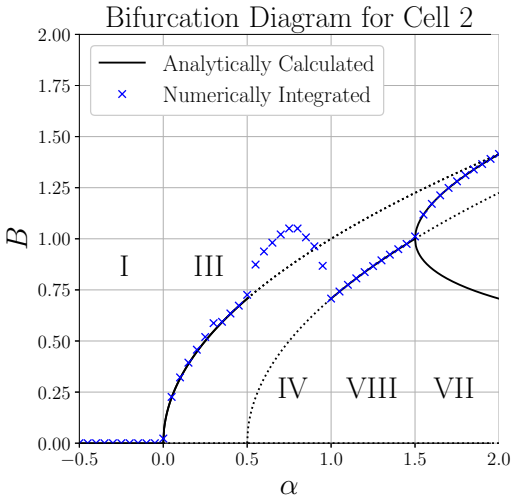

FIG. 9: Bifurcation diagram for the second cell in a three-cell feedforward network with self-coupling and unforced input. Parameters are: $\Phi = \pi/3$, $\kappa = 1$.

Now, consider Region IV. This is probably the most interesting region for cell 2. Without going into too much detail, multifrequency behavior arising out of a torus bifurcation and disappearing in a saddle node is found in this region. Interesting patterns of oscillations, possibly chaotic for some parameter values, and transition from fast oscillations to slow oscillations, are also observed. A complete analysis of this region is beyond the scope of the present work.

Traversing horizontally across Region IV (along a fixed value of Φ with increasing α) can give rise to different behaviors. One may traverse from Region IV to Region V, or IV to VIII, or IV directly to X through a codimension-two bifurcation. Consider Region V. In this region, cells one and two appear to be phase-locked. That is, they oscillate with the same frequency but out of phase with each other by a fixed amount. Equation (30) indicates that, within Region V, cell two has a larger amplitude along Branch 2 and 3, as is shown in Fig. 10. Consider

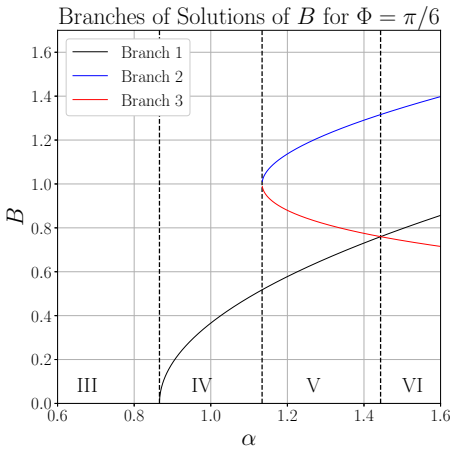

FIG. 10: Branches of solutions of B for $\Phi = \pi/6$ and $\kappa = 1$, as defined in Eq. (30). Vertical dashed lines represent the borders of Regions III, IV, V, and VI. Notice that the border between Region V and VI is defined to be the point where Branches 1 and 3 cross.

Region VI. This region is qualitatively similar to Region V. The difference is the crossing of Branch 3 and Branch 1 of Eq. (30). That is, Branch 1 now shows a larger amplitude than that of Branch 3.

Region VII also appears to consist of phase-locked oscillations between cells one and two. The boundary between Region VII and Region IX is marked by the boundary between complete synchronization and phase locked solutions. Consider Region VIII. This region is qualitatively similar to Region II. The only difference is the appearance of an additional unstable equilibrium point at $A = 0$, $B = \sqrt{\alpha}$, see Fig. 11.

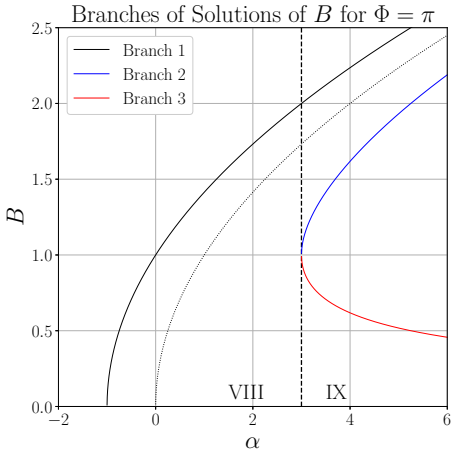

FIG. 11: Branches of solutions of B for $\Phi = \pi$ and $\kappa = 1$, as defined in Eq. (30). Vertical dashed line represents the boundary of Regions VIII and IX. The dotted curve is the unstable solution $B = \sqrt{\alpha}$.

Consider Region IX. This region is qualitatively similar to Region VIII, with the onset of additional solu-

tions along the stable branch of $A = \sqrt{\alpha - \kappa\cos\Phi}$, which arise via a saddle node bifurcation. We have shown that Branch 1 is always stable in this region. Numerical computations of the eigenvalues of J along Branch 2 in this region show that it is a stable branch, while Branch 3 is unstable in this region. Consider Region X. In this region, bistability between the synchronization state and a phase-locked solution is found.

3. *Third Cell*

Continuing the analysis for the third cell, we get from Eq. (19) the following amplitude and phase dynamics

$$\begin{aligned} C' &= \alpha C - C^3 - \kappa B\cos(\Phi - (\phi_3 - \phi_2)) \\ C\phi_3' &= \kappa C\sin\Phi - \kappa B\sin(\Phi - (\phi_3 - \phi_2)). \end{aligned} \tag{31}$$

Equation (31) is again an asymptotically autonomous system. The differential equations in (31) depend on the quantity $\phi_3 - \phi_2$. Thus, let us consider solutions from Region III, with $\theta = \phi_3 - \phi_2$. Combining Eq. (23) and Eq. (31) we arrive at

$$\begin{aligned} C' &= \alpha C - C^3 - \kappa B\cos(\Phi - \theta) \\ \theta' &= -\kappa\frac{B}{C}\sin(\Phi - \theta). \end{aligned} \tag{32}$$

We can see that under the assumptions $B > 0$ and $C > 0$, Eq. (32) has $\theta = \Phi$ as an unstable fixed point and $\theta = \Phi \pm \pi$ as stable equilibrium points (as well as infinitely many others). Without loss of generality, we assume $\theta = \Phi + \pi$ as a representative for a stable equilibrium point, which we can substitute into the first equation of Eq. (32), which causes it to decouple and become

$$C' = \alpha C - C^3 + \kappa B. \tag{33}$$

We use $B = \sqrt{\alpha}$ and substitute this solution into Eq. (33) to get the equation of the equilibrium point

$$\alpha C - C^3 + \kappa\sqrt{\alpha} = 0. \tag{34}$$

From previous work [12], we know that this equation shows the 1/6th power growth rate. Indeed, Fig. 12 shows a stable branch of a Hopf bifurcation displaying the 1/6th power growth rate starting at the origin, but, interestingly, there is a similar bifurcation as the oscillator bifurcates at the boundary of Region V.

B. Synchronization and Phase Locking

We now investigate in more detail the existence and stability of the synchronization state (same amplitude of oscillations and same phase) as well as the phase-locking state in which the cells oscillate with a constant phase difference but the amplitudes may vary. We start with

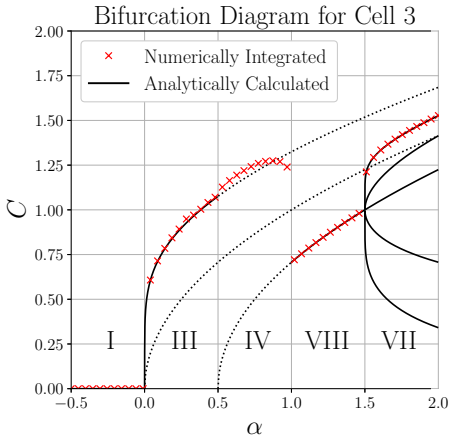

FIG. 12: Bifurcation diagram for the third cell in a three-cell feedforward network with self-coupling and unforced input. In Region III, the third cell exhibits 1/6th power growth rate, which is significantly larger than the standard square-root growth rate found in individual oscillators that undergo Hopf bifurcations. Parameters are: $\Phi = \pi/3$, $\kappa = 1$.

the case of $N = 3$ cells and then generalize the results to larger networks.

As it turns out, the synchronization of cell three with cells two and one follows the same process as the synchronization of cell two with one. That is, let's assume $\alpha - \kappa\cos\Phi > 0$, so that cells two and one are synchronized at the stable amplitude $B = A = \sqrt{\alpha - \kappa\cos\Phi}$. Substituting this amplitude into Eq. (31) yields

$$\begin{aligned} C' &= \alpha C - C^3 - \kappa\sqrt{\alpha - \kappa\cos\Phi}\cos(\Phi - \theta) \\ C\phi_3' &= \kappa C\sin\Phi - \kappa\sqrt{\alpha - \kappa\cos\Phi}\sin(\Phi - \theta). \end{aligned} \tag{35}$$

Observe that if we replace θ with ϕ_2 and C with B in Eq. (35), then we obtain Eq. (26). This means that the synchronization of cell three with two and one is governed by the same type of dynamics as that of the synchronization between cells two and one. It follows that (C^*, θ^*) is an equilibrium point of Eq. (35), where

$$C^* = \sqrt{\alpha - \kappa\cos\Phi}, \qquad \theta* = 0.$$

Since we know that $\phi_2 = 0$ then $\phi_3 = 0$. Consequently, the linearization of Eq. (35) about the equilibrium (C^*, θ^*) leads to the same region of parameter space, (α, Φ), where the synchronization state between cells three and two and one is stable. Figure 13 illustrates the synchronization of the three cells for a choice of parameters within Region VIII. The observed low-frequency of oscillations is due to the small denominator, $\omega = \omega_0 - \varepsilon\kappa\sin\Phi$.

The mechanism that leads to synchronization between the three cells also applies to larger feedforward network. That is, as the number of cells increases, the dynamics for cell k, with $k > 3$, is governed by an asymptotically autonomous system that depends on the long-term behavior

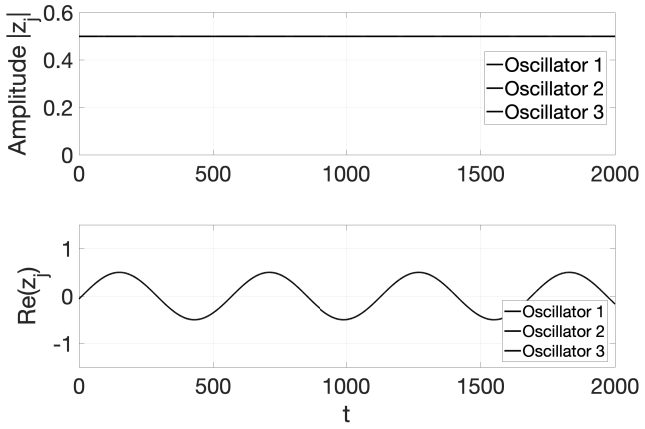

FIG. 13: Synchronization in a three-cell feedforward network, with long periods of oscillations. Parameters are: $\alpha = 0.1$, $\Phi = \pi/2 + 0.15$, $\omega_0 = 1$, $\kappa = 1$.

of cell $k-1$. Since the amplitude of cell $k-1$ always converges to an equilibrium point, the dependence of cell k on $k-1$ vanishes, so we can substitute its long-term behavior into the governing equations for cell k. The result is a system of equations of the same form as Eq. (35). This system of equations leads to the same region of parameter space, (α, Φ), where the synchronization state exists and is stable.

We now consider the existence and stability of phase-locked oscillations in larger arrays. We would like to emphasize that this type of solution is different from the synchronization states in the sense that it does not require for the amplitudes to be identical. That is, individual cells can oscillate with their own unique (possibly different) amplitude but with the same phase difference. Next, we prove an important conclusion: phase-locking is a stable solution in a feedforward network. The proof is valid for an arbitrary large network of oscillators.

Lemma 1. *Consider a feed forward network with self coupling, given by Eq. (13), with N identical nodes. Assume that an asymptotic analysis leads to a set of nonlinear amplitude-phase equations of the form*

$$\begin{aligned} \dot{A}_j &= f(A_j, A_{j-1}, \Phi, \phi_j, \phi_{j-1}) \\ \dot{\phi}_j &= g(A_j, A_{j-1}, \Phi, \phi_j, \phi_{j-1}), \end{aligned} \tag{36}$$

where $j = 1, \ldots, N$. Let $\theta_j = \phi_j - \phi_{j-1}$ for each $j > 1$. Then if $\Phi \pm \pi$ are stable equilibria of θ_j, then $\Phi \pm \pi$ are also stable equilibria of θ_{j+1}.

Proof. For cells j and $j+1$ we have (non-negative) amplitudes A_j and A_{j+1} respectively, and phases ϕ_j and ϕ_{j+1} respectively, satisfying the following system of differential equations:

$$\begin{aligned} A_j' &= \alpha A_j - A_j^3 - \kappa A_{j-1}\cos(\Phi - (\phi_j - \phi_{j-1})) \\ A_j\phi_j' &= \kappa A_j \sin\Phi - \kappa A_{j-1}\sin(\Phi - (\phi_j - \phi_{j-1})) \\ A_{j+1}' &= \alpha A_{j+1} - A_{j+1}^3 - \kappa A_j\cos(\Phi - (\phi_{j+1} - \phi_j)) \\ A_{j+1}\phi_{j+1}' &= \kappa A_{j+1}\sin\Phi - \kappa A_j\sin(\Phi - (\phi_{j+1} - \phi_j)). \end{aligned} \tag{37}$$

It follows that

$$\theta_{j+1}' = \kappa\frac{A_{j-1}}{A_j}\sin(\Phi - \theta_j) - \kappa\frac{A_j}{A_{j+1}}\sin(\Phi - \theta_{j+1}), \tag{38}$$

where $\theta_{j+1} = \phi_{j+1} - \phi_j$. But by assumption, $\theta_j \to \Phi \pm \pi$ so that the first term vanishes (by Wiggins 17.0.3). We are left with

$$\theta_{j+1}' = \kappa\frac{A_j}{A_{j+1}}\sin(\theta_{j+1} - \Phi). \tag{39}$$

Since we have required $A_j \geq 0$ for all j, we can see that $\theta_{j+1} = \Phi$ is an unstable equilibrium, while $\theta_{j+1} = \Phi \pm \pi$ are stable equilibria (of course there are infinitely many others). □

Figure 14 illustrates phase-locking in a feedforward network with ten nodes. Observe that the amplitudes. are, however, different. Thus the system does not exhibit synchronization, but only phase locking.

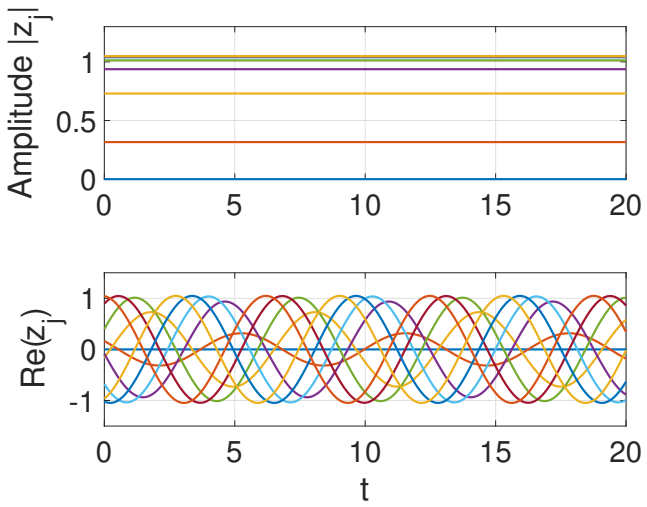

FIG. 14: Phase-locking oscillations in a ten-cell feedforward network, with $\Phi = \pi/10$. Note that this is not a traveling wave solution induced by symmetry; it is a constant phase difference chosen to match the number of oscillators.

The significance of this result is that it shows that a constant phase difference, $\theta_j = \Phi \pm \pi$, between consecutive oscillators is stable behavior, and that the same phase difference can be exploited for beam steering, and, simultaneously, for signal amplification. Since $\Phi - \pi \equiv \Phi + \pi \pmod{2\pi}$, we can assume, without loss of generality

the stable equilibrium to be $\Phi+\pi$. Then, we can rewrite the array factor as a function of Ψ and Φ as follows

$$A(\Psi+\Phi)=\frac{\sin\left(\dfrac{N(\Psi+\Phi\pm\pi)}{2}\right)}{N\sin\left(\dfrac{\Psi+\Phi\pm\pi}{2}\right)}e^{i(N-1)(\Psi+\Phi\pm\pi)/2}. \tag{40}$$

The derivation of the array factor formula assumes that all amplitudes are identical. That happens in our analysis and simulations, as it can be observed from Fig. 14, after cell 3. Thus, we can disregard the oscillations of the first two cells, since their dynamics has already lead to the signal amplification effect, while taking advantage of the constant phase difference among the remaining cells.

IV. FEEDFORWARD NETWORK WITHOUT SELF COUPLING

We now consider a feedforward network, which is very similar to that of the model Eq. (13), except that this time the self-coupling term on the first cell is being dropped. An advantage of this approach is that the amplitude-equations simplify slightly enough so that analysis is more amenable. More importantly, the phase dynamics depends directly on the phase differences among consecutive oscillators, and such phase difference can be readily used for beam steering purposes. The model equations take the form:

$$\begin{aligned}\dot{z}_1 &= (\alpha+\omega_1 i)\,z_1-|z_1|^2z_1,\\ \dot{z}_j &= (\alpha+\omega_j i)\,z_j-|z_j|^2z_j-\kappa e^{i\Phi}z_{j-1}.\end{aligned} \tag{41}$$

Next we conduct an asymptotic analysis, similar to the self-coupling case, to investigate in more detail the nature of the bifurcations and the amplitude response of the oscillators.

A. Signal Amplification

Once again, to get insight into the collective behavior of the network Eq. (41), we consider first the special case of $N=3$ oscillators. We write the model equations in the usual form:

$$\begin{aligned}\dot{x}&=(\alpha+i\omega_0)x-|x|^2x\\ \dot{y}&=(\alpha+i\omega_0)y-|y|^2y-\kappa e^{i\Phi}x\\ \dot{z}&=(\alpha+i\omega_0)z-|z|^2z-\kappa e^{i\Phi}y.\end{aligned} \tag{42}$$

Using the same two-time scale analysis of Section III, we seek asymptotic expansions for x, y, and z in a truncated series of ε of the form

$$\begin{aligned}x&=x_0+\varepsilon x_1+\varepsilon^2x_2+\cdots\\ y&=y_0+\varepsilon y_1+\varepsilon^2y_2+\cdots\\ z&=z_0+\varepsilon z_1+\varepsilon^2z_2+\cdots.\end{aligned} \tag{43}$$

Substituting Eq. (43) into Eq. (42), and using the chain rule, produces, after collecting equal powers of ε, a set of partial differential equations (not shown for brevity) for each order term. The solutions of the PDEs yields

$$\begin{aligned}x_0&=A(\eta)e^{i(\xi+\phi_1(\eta))}\\ y_0&=B(\eta)e^{i(\xi+\phi_2(\eta))}\\ z_0&=C(\eta)e^{i(\xi+\phi_3(\eta))},\end{aligned} \tag{44}$$

where $\xi=\omega t$ represents the fast time scale of the system, while $\eta=\varepsilon t$ is the slow time scale. The amplitudes A, B and C are governed by the following slow-time amplitude and phase equations

$$\begin{aligned}A'&=\alpha A-A^3\\ B'&=\alpha B-B^3-\kappa A\cos(\Phi+\phi_1-\phi_2)\\ C'&=\alpha C-C^3-\kappa B\cos(\Phi+\phi_2-\phi_3)\\ \phi_1'&=0\\ \phi_2'&=-\kappa\frac{A}{B}\sin(\Phi+\phi_1-\phi_2)\\ \phi_3'&=-\kappa\frac{B}{C}\sin(\Phi+\phi_2-\phi_3).\end{aligned} \tag{45}$$

Observe that this time the amplitude dynamics for the first cell, A, is independent of the phase coupling variable Φ. Furthermore, the amplitude A undergoes a pitchfork bifurcation at $\alpha=0$, leading to one trivial solution, $A=0$, and two nontrivial equilibrium solutions $A=\pm\sqrt{\alpha}$. For values of $\alpha>0$, the trivial solution is unstable, while the nontrivial solutions are locally stable whenever they exist. This observation is important because in the self-coupled system the bifurcations on the first cell were dependent on both, α and Φ, while now, the bifurcation occurs independently of Φ.

Observe also that the phase dynamics in cells two and three depends on the phase difference with respect to the preceeding oscillators. Thus, we define, $\theta_j=\phi_j-\phi_{j-1}$, for $j>1$, and rewrite the phase difference dynamics as

$$\begin{aligned}\theta_2'&=\kappa\frac{A}{B}\sin(\theta_2-\Phi)\\ \theta_3'&=\kappa\frac{C}{B}\sin(\theta_3-\Phi)-\kappa\frac{A}{B}\sin(\theta_2-\Phi).\end{aligned} \tag{46}$$

From the first equation in (46), we see that $\theta_2=\Phi\pm\pi$ is a stable equilibrium. Since $\Phi-\pi\equiv\Phi+\pi\ (\mathrm{mod}\ 2\pi)$, we can assume, without loss of generality the stable equilibrium to be $\Phi+\pi$. By substituting $\theta_2=\Phi+\pi$ into the second equation in (46), we find that $\theta_3=\Phi+\pi$ is also a stable equilibrium. It follows then that $\phi_2=\phi_1+\Phi+\pi$

and that $\phi_3 = \phi_2 + \Phi + \pi$. Hence, we have found a constant phase difference between the oscillators.

Using $\theta_2 = \phi_2 - \phi_1$, we may recast the amplitude dynamics for the second cell in Eq. (45), to get

$$B' = \alpha B - B^3 - \kappa A \cos(\Phi - \theta_2). \tag{47}$$

Substituting the stable equilibrium value $\theta_2 = \Phi + \pi$ into Eq. (47) gives

$$B' = \alpha B - B^3 + \kappa A.$$

We have shown in previous work, see Theorem 1 in [12], that when $\kappa = 1$ and $A = \sqrt{\alpha}$, then cell B has a branch of stable equilibria with a growth rate of $\alpha^{1/6}$. Similarly, we find

$$C' = \alpha C - C^3 + \kappa B.$$

Since B has already undergone a growth rate of $\alpha^{1/6}$, then, this time, C will experience growth as $\alpha^{1/18}$. The important fact is that the bifurcations along both branches, B and C, have now led us to signal amplification. Furthermore, these larger growth rates can be exploited for beam steering purposes, just as we showed in the previous section. Next, we address the issue of phase locking, which can be used, precisely, to steer a beam at a desired angle.

B. Phase Locking

In this section we consider again the existence and stability of phase locking solutions among arbitrarily large networks of oscillators. We prove, as in the case of feedforward networks with self-coupling, that phase-locking solutions are also stable. This result allows for the possibility of achieving signal amplification and beam steering in a simpler feedforward network. That is, in a network that would not require self-coupling. The main result is expressed through the following lemma.

Lemma 2. *Consider a feed forward network with self coupling, given by Eq. (13), with N identical nodes. Assume that an asymptotic analysis leads to a set of nonlinear amplitude-phase equations of the form*

$$\begin{aligned} \dot{A}_j &= f(A_j, A_{j-1}, \Phi, \phi_j, \phi_{j-1}) \\ \dot{\phi}_j &= g(A_j, A_{j-1}, \Phi, \phi_j, \phi_{j-1}), \end{aligned} \tag{48}$$

where $j = 1, \ldots, N$. Let $\theta_j = \phi_j - \phi_{j-1}$ for each $j > 1$. Then if $\Phi \pm \pi$ are stable equilibria of θ_j, then $\Phi \pm \pi$ are also stable equilibria of θ_{j+1}.

Proof. For cells j and $j+1$ we have (non-negative) amplitudes A_j and A_{j+1} respectively, and phases ϕ_j and ϕ_{j+1} respectively, satisfying the following system of differential equations:

$$\begin{aligned} A_1' &= \alpha A_1 - A_1^3 \\ A_1\phi_1' &= 0 \\ A_j' &= \alpha A_j - A_j^3 - \kappa A_{j-1}\cos(\Phi - (\phi_j - \phi_{j-1})) \\ A_j\phi_j' &= -\kappa A_{j-1}\sin(\Phi - (\phi_j - \phi_{j-1})) \\ A_{j+1}' &= \alpha A_{j+1} - A_{j+1}^3 - \kappa A_j\cos(\Phi - (\phi_{j+1} - \phi_j)) \\ A_{j+1}\phi_{j+1}' &= -\kappa A_j\sin(\Phi - (\phi_{j+1} - \phi_j)). \end{aligned} \tag{49}$$

It follows that

$$\theta_{j+1}' = \kappa\frac{A_{j-1}}{A_j}\sin(\Phi - \theta_j) - \kappa\frac{A_j}{A_{j+1}}\sin(\Phi - \theta_{j+1}), \tag{50}$$

where $\theta_{j+1} = \phi_{j+1} - \phi_j$. But by assumption, $\theta_j \to \Phi \pm \pi$ so that the first term vanishes (by Wiggins 17.0.3). We are left with

$$\theta_{j+1}' = \kappa\frac{A_j}{A_{j+1}}\sin(\theta_{j+1} - \Phi). \tag{51}$$

Since we have required $A_j \geq 0$ for all j, we can see that $\theta_{j+1} = \Phi$ is an unstable equilibrium, while $\theta_{j+1} = \Phi \pm \pi$ are stable equilibria (of course there are infinitely many others). □

Since the constant phase difference among consecutive oscillators is stable, we can, once again, apply this phase difference to steer the beam. That is, the substitution of θ_j into the array factor and the resulting Eq. (40) is still valid for a feedforward network without self coupling.

V. DISCUSSION

Studies of active antennas and radar systems involve two main issues. The transmission problem, which includes generating and steering a radiating beam pattern in a desired direction, and, the reception problem, which involves understanding the response of the beamformer to incident signals. Part I of this manuscript was dedicated to the transmission problem. More specifically, we have shown that the amplitudes of certain bifurcating solutions in a feedforward network of nonlinear oscillators exhibit growth rates that are significantly larger than in other type of networks that operate near the onset of a Hopf bifurcation. Those branches of oscillations have the potential to lead to significant signal amplification of a radiating beam. In addition, the bifurcation of such solutions also exhibit stable phase-locking patterns of collective oscillations, in which the phase difference among consecutive oscillators is constant. Those phase differences are critical to steer a beam towards a desired location. Together, the larger growth rate of the amplitudes of the oscillations and the phase-locking characteristics, provide innovative solutions, and improvements (e.g., simultaneous signal amplification and beam steering ca-

pabilities) over conventional methods, for addressing the transmission problem. In part II of the manuscript, we will address the reception problem. That is, we will study the response of the nonlinear feedforward network to incident signals.

ACKNOWLEDGEMENTS

We gratefully acknowledge support from the Office of Naval Research (Code 332) and NIWC Pacific internal S&T program. A.P. was supported by a Grant from the Naval Information Warfare Center (NIWC) Pacific, San Diego.

A. Two-Time Scale Analysis of Feedforward Network with Self-Coupling

For completeness purposes, we re-write the network equations as

$$\begin{aligned}\dot{x} &= (\varepsilon\alpha + i\omega_0)x - \varepsilon|x|^2x - \varepsilon\kappa e^{i\Phi}x\\ \dot{y} &= (\varepsilon\alpha + i\omega_0)y - \varepsilon|y|^2y - \varepsilon\kappa e^{i\Phi}x\\ \dot{z} &= (\varepsilon\alpha + i\omega_0)z - \varepsilon|z|^2z - \varepsilon\kappa e^{i\Phi}y.\end{aligned} \tag{A1}$$

We introduce two time scales: a fast time, $\xi = \omega t$, and a slow time $\eta = \varepsilon t$, where

$$\omega = \omega_0 - \varepsilon\kappa\sin\Phi.$$

Applying the chain rule we arrive at

$$\frac{d}{dt} = \omega_0\frac{\partial}{\partial\xi} - \varepsilon\kappa\sin\Phi\frac{\partial}{\partial\xi} + \varepsilon\frac{\partial}{\partial\eta}.$$

We seek an asymptotic expansion of the solutions x, y and z as a truncated series of ε

$$\begin{aligned}x &= x_0 + \varepsilon x_1 + \varepsilon^2x_2 + \cdots\\ y &= y_0 + \varepsilon y_1 + \varepsilon^2y_2 + \cdots\\ z &= z_0 + \varepsilon z_1 + \varepsilon^2z_2 + \cdots.\end{aligned} \tag{A2}$$

Substituting Eq. (A2) into Eq. (A1), and using the chain rule above, produces, up to order $\mathcal{O}(\varepsilon)$, the following set of partial differential equations (PDE)

$$\begin{aligned}&\omega_0\frac{\partial x_0}{\partial\xi} - \varepsilon\kappa\sin\Phi\frac{\partial x_0}{\partial\xi} + \varepsilon\frac{\partial x_0}{\partial\eta} + \varepsilon\omega_0\frac{\partial x_1}{\partial\xi} =\\ &\varepsilon\alpha x_0 + i\omega_0x_0 + i\varepsilon\omega_0x_1 - \varepsilon|x_0|^2x_0 - \varepsilon\kappa e^{i\Phi}x_0\\ &\omega_0\frac{\partial y_0}{\partial\xi} - \varepsilon\kappa\sin\Phi\frac{\partial y_0}{\partial\xi} + \varepsilon\frac{\partial y_0}{\partial\eta} + \varepsilon\omega_0\frac{\partial y_1}{\partial\xi} =\\ &\varepsilon\alpha y_0 + i\omega_0y_0 + i\varepsilon\omega_0y_1 - \varepsilon|y_0|^2y_0 - \varepsilon\kappa e^{i\Phi}x_0\\ &\omega_0\frac{\partial z_0}{\partial\xi} - \varepsilon\kappa\sin\Phi\frac{\partial z_0}{\partial\xi} + \varepsilon\frac{\partial z_0}{\partial\eta} + \varepsilon\omega_0\frac{\partial z_1}{\partial\xi} =\\ &\varepsilon\alpha z_0 + i\omega_0z_0 + i\varepsilon\omega_0z_1 - \varepsilon|z_0|^2z_0 - \varepsilon\kappa e^{i\Phi}y_0.\end{aligned} \tag{A3}$$

Eliminating $\mathcal{O}(1)$ terms, we get a system of equations for x_0, y_0, and z_0:

$$\begin{aligned}\frac{\partial x_0}{\partial\xi} &= ix_0\\ \frac{\partial y_0}{\partial\xi} &= iy_0\\ \frac{\partial z_0}{\partial\xi} &= iz_0,\end{aligned} \tag{A4}$$

with solutions

$$\begin{aligned}x_0 &= A(\eta)e^{i(\xi+\phi_1(\eta))}\\ y_0 &= B(\eta)e^{i(\xi+\phi_2(\eta))}\\ z_0 &= C(\eta)e^{i(\xi+\phi_3(\eta))}.\end{aligned} \tag{A5}$$

Now we consider $\mathcal{O}(\varepsilon)$ terms.

$$\begin{aligned}\omega_0\frac{\partial x_1}{\partial\xi} &= i\omega_0x_1 - \frac{\partial x_0}{\partial\eta} + \kappa\sin\Phi\frac{\partial x_0}{\partial\xi} + \alpha x_0 -\\ &\quad |x_0|^2x_0 - \kappa e^{i\Phi}x_0\\ \omega_0\frac{\partial y_1}{\partial\xi} &= i\omega_0y_1 - \frac{\partial y_0}{\partial\eta} + \kappa\sin\Phi\frac{\partial y_0}{\partial\xi} + \alpha y_0 -\\ &\quad |y_0|^2y_0 - \kappa e^{i\Phi}x_0\\ \omega_0\frac{\partial z_1}{\partial\xi} &= i\omega_0z_1 - \frac{\partial z_0}{\partial\eta} + \kappa\sin\Phi\frac{\partial z_0}{\partial\xi} + \alpha z_0 -\\ &\quad |z_0|^2z_0 - \kappa e^{i\Phi}y_0.\end{aligned} \tag{A6}$$

Requiring secular terms to vanish, we have

$$\begin{aligned}\frac{\partial x_0}{\partial\eta} &= \kappa\sin\Phi\frac{\partial x_0}{\partial\xi} + \alpha x_0 - |x_0|^2x_0 - \kappa e^{i\Phi}x_0\\ \frac{\partial y_0}{\partial\eta} &= \kappa\sin\Phi\frac{\partial y_0}{\partial\xi} + \alpha y_0 - |y_0|^2y_0 - \kappa e^{i\Phi}x_0\\ \frac{\partial z_0}{\partial\eta} &= \kappa\sin\Phi\frac{\partial z_0}{\partial\xi} + \alpha z_0 - |z_0|^2z_0 - \kappa e^{i\Phi}y_0.\end{aligned} \tag{A7}$$

To extract the amplitude dynamics of just the first cell in the network, we substitute Eq. (A5) into the first equation of Eq. (A7). Using the notation $(\cdot)'$ to mean ∂_η, we get

$$A' + iA\phi_1' = i\kappa A\sin\Phi + \alpha A - A^3 - \kappa A\cos\Phi - i\kappa A\sin\Phi. \tag{A8}$$

Separating real and imaginary parts of Eq. (A8), we get

$$\begin{aligned}A' &= (\alpha - \kappa\cos\Phi)A - A^3\\ A\phi_1' &= 0.\end{aligned} \tag{A9}$$

Now we consider the second equation from Eq. (A7).

Recalling that $\phi_1 = 0$, we have

$$\omega_0 \frac{\partial y_1}{\partial \xi} = i\omega_0 y_1 - \frac{\partial y_0}{\partial \eta} + \kappa \sin\Phi \frac{\partial y_0}{\partial \xi} + \alpha y_0 - |y_0|^2 y_0 - \kappa e^{i\Phi} A e^{i\xi}. \quad \text{(A10)}$$

Requiring resonant terms to vanish in Eq. (A10), we have

$$\frac{\partial y_0}{\partial \eta} = \kappa \sin\Phi \frac{\partial y_0}{\partial \xi} + \alpha y_0 - |y_0|^2 y_0 - \kappa e^{i\Phi} A e^{i\xi}. \quad \text{(A11)}$$

Substituting Eq. (A5) into Eq. (A11), we have

$$B' + i\phi_2' B = i\kappa B \sin\Phi + \alpha B - B^3 - \kappa A \cos(\Phi - \phi_2) - i\kappa A \sin(\Phi - \phi_2). \quad \text{(A12)}$$

Separating real and imaginary parts, we have

$$\begin{aligned} B' &= \alpha B - B^3 - \kappa A \cos(\Phi - \phi_2) \\ B\phi_2' &= \kappa B \sin\Phi - \kappa A \sin(\Phi - \phi_2). \end{aligned} \quad \text{(A13)}$$

Continuing the analysis for the third cell, we proceed as before. After substituting the Ansatz solutions from Eq. A5 into Eq. A3, and letting the secular terms vanish, we arrive at

$$C' + i\phi_3' C = i\kappa C \sin\Phi + \alpha C - C^3 - \kappa B \cos(\Phi - (\phi_3 - \phi_2)) - i\kappa B \sin(\Phi - (\phi_3 - \phi_2)). \quad \text{(A14)}$$

Separating real and imaginary parts, we get

$$\begin{aligned} C' &= \alpha C - C^3 - \kappa B \cos(\Phi - (\phi_3 - \phi_2)) \\ C\phi_3' &= \kappa C \sin\Phi - \kappa B \sin(\Phi - (\phi_3 - \phi_2)). \end{aligned} \quad \text{(A15)}$$

[1] T. Heath, K. Wiesenfeld, and R. York, Int. J. Bif. Chaos **10**, 2619 (2000).
[2] R. Hansen, *Phased Array Antennas* (John Wiley & Sons, Inc., 2009).
[3] K. Stephan, IEEE Trans. Microwave Theory Tech. **MTT-34**, 1017 (1986).
[4] K. Stephan and W. Morgan, IEEE Trans. Antennas Propagat **AP-35**, 771 (1987).
[5] R. York and T. Itoh, IEEE Trans. Microwave Theory Tech. **46**, 1920 (1998).
[6] R. York, IEEE Trans. Microwave Theory Tech. **41**, 1799 (1993).
[7] B. Meadows, T. Heath, J. Neff, E. Brown, D. Fogliatti, M. Gabbay, V. In, P. Hasler, S. Deweerth, and W. Ditto, Proc. of the IEEE **90**, 882 (2002).
[8] M. Gabbay, M. Larsen, and L. Tsimring, Proc. SPIE, Advanced Signal Processing Algorithms, Architectures, and Implementations XIV **5559**, 146 (2004).
[9] T. Elmhirst and M. Golubitsky, J. Applied Dynamical Systems **5**, 205 (2006).
[10] M. Golubitsky, M. Nicol, and I. Stewart, J. Nonlinear Sci. **14**, 207 (2004).
[11] M. Golubitsky and C. Postlethwaite, Discrete and Continuous Dynamical Systems **32**, 2913 (2012).
[12] T. Levasseur and A. Palacios, Int. J. Bif. Chaos **In Print** (2000).
[13] S. Wiggins, *Introduction to Applied Nonlinear Dynamical Systems* (Springer-Verlag, New York, 1990).
[14] A. Nayfeh, *The Method of Normal Forms* (Wiley-VCH, 2011).
[15] M. Golubitsky, L. Shiau, C. Postlethwaite, and Y. Zhang, in *Coherent Behavior in Neuronal Networks*, edited by K. J. et al. (Springer Science+Business Media, LLC, 2009).
[16] N. McCullen, T. Mullin, and M. Golubitsky, Physical Review Letters **98** (2007).
[17] B. Rink and J. Sanders, Trans. Amer. Math. Soc. **367**, 3509 (2015).
[18] Y. Zhang and M. Golubitsky, SIAM J. Applied Dynamical Systems **10**, 1272 (2011).
[19] I. Stewart and M. Golubitsky, SIAM J. Appl. Dynamical Systems **10**, 1404 (2011).
[20] I. Stewart and M. Golubitsky, SIAM J. Appl. Dynamical Systems **13**, 129 (2014).